First-principles hybrid functional study of the electronic structure and charge carrier mobility in perovskite $CH_3NH_3SnI_3$*

Li-Juan Wu(伍丽娟)[1], Yu-Qing Zhao(赵宇清)[1], Chang-Wen Chen(陈畅文)[2], Lin-Zhi Wang(王琳芝)[1], Biao Liu(刘标)[1], and Meng-Qiu Cai(蔡孟秋)[1,†]

[1] *School of Physics and Electronics Science, Hunan University, Changsha* 410082, *China*
[2] *Yali Middle School, Changsha* 410007, *China*

(Received 25 March 2016; revised manuscript received 1 June 2016; published online 25 August 2016)

We calculate the electronic properties and carrier mobility of perovskite $CH_3NH_3SnI_3$ as a solar cell absorber by using the hybrid functional method. The calculated result shows that the electron and hole mobilities have anisotropies with a large magnitude of 1.4×10^4 $cm^2 \cdot V^{-1} \cdot s^{-1}$ along the y direction. In view of the huge difference between hole and electron mobilities, the perovskite $CH_3NH_3SnI_3$ can be considered as a p-type semiconductor. We also discover a relationship between the effective mass anisotropy and electronic occupation anisotropy. The above results can provide reliable guidance for its experimental applications in electronics and optoelectronics.

Keywords: charge carrier mobility, nontoxic perovskite, solar cell absorber, HSE06 calculations, effective masses anisotropy

PACS: 72.20.Jv, 82.47.Jk, 71.20.–b, 88.05.Tg **DOI:** 10.1088/1674-1056/25/10/107202

1. Introduction

The recent emergence of halide perovskites as light harvesters and transport materials has revolutionized the scenario of emerging photovoltaic technologies. Organic–inorganic hybrid perovskite based on metal halides adopts the ABX_3 perovskite structure (B cation = Sn^{2+} or Pb^{2+}; X is typically Br^{1-}, or I^{1-}; and the A cation is selected to balance the total charge and it is a small organic cation) solar cells are revolutionizing the field because of the potential for high efficiency and long dispersion length.[1–5] Therefore, in order to realize the sustainable development of energy and commercialization of technology, it is necessary to reach analogous optical and photovoltaic performance developing environmentally friendly solar cells. As is well known, lead poisoning is a type of metal poisoning and does harm to both the human body and the natural environment.[6] Motivated by non-toxic atoms of Sn in the same group compared with Pb, one substituted Sn^{2+} for Pb^{2+}. However, a recent study[7] has reported that the strong acidification induced by the SnI_2 is found to be more harmful than the combined effect of milder acidification and the expected Pb intoxication induced by PbI_2, indicating that Sn-based perovskite may not be the ideal Pb surrogate. Fortunately, our experimental group has substituted Ge for Pb and Sn, considering this problem, tuning the superior solar cell performance of effective mass and absorption in perovskite $CH_3NH_3GeCl_3$ under hydrostatic pressure.[8] Recent implementation of $CH_3NH_3SnI_3$ (X = Cl, Br, I) perovskite absorbers enabled power conversion efficiency of 12%–15%, which has been recognized as "The Next Big Thing in Photovoltaics". This makes them a possible light absorber in energy conversion or detector devices.[2] The perovskite $CH_3NH_3SnI_3$ has an optical band gap of 1.3 eV,[9] indicating a significant red shift compared with the $CH_3NH_3PbI_3$ (about 1.55 eV).[10]

Recently, lead-free solid-state organic–inorganic hybrid halide perovskite solar cells based on methylammonium tin iodide perovskite semiconductor as the light harvester, such as $CH_3NH_3SnI_3$, has been identified as a promising photovoltaic (PV) material.[2] Bandgap engineering was implemented by chemical substitution in the form of $CH_3NH_3SnI_{3-x}Br_x$ solid solutions, which can be controllably tuned to cover much of the visible spectrum, thus enabling the realization of lead-free solar cells with an initial power conversion efficiency of 5.73% under simulated full sunlight.[9] Thus, many studies have focused on $CH_3NH_3SnX_3$. For example, Lang *et al.*[11] studied the chemical trends of the electronic properties in halide perovskites and proposed that $CH_3NH_3SnBr_3$ could be a promising light-harvesting material because of appropriate band gap and optical absorption. Feng *et al.*[12] reported that the band gaps of $CH_3NH_3SnX_3$ can be engineered to match the visible light spectrum under the low hydrostatic pressure (including compression and expansion). Umari *et al.* predicted that $CH_3NH_3SnI_3$ has better electron transport properties than $CH_3NH_3PbI_3$.[13] The efficiency is expected to be further increased by optimizing and better fundamental understanding

*Project supported by the National Natural Science Foundation of China (Grant No. 51172067), the Hunan Provincial Natural Science Fund for Distinguished Young Scholars, China (Grant No. 13JJ1013), the Specialized Research Fund for the Doctoral Program of Higher Education, China (Grant No. 20130161110036), and the New Century Excellent Talents in University, China (Grant No. NCET-12-0171.D).

†Corresponding author. E-mail: mqcai@hnu.edu.cn

of the internal electron dynamics and corresponding interfacial engineering. Papaassiliou and Koutselas[10] reported that perovskite solar cells represent a step towards the realization of low-cost, environmentally friendly solid-state solar cells. Despite prosperous applications of the Sn-based hybrid perovskites in solar cells, a systematic fundamental understanding of their electronic properties and band-edge positions is important for further optimizing their material properties. Jia *et al.*[14] reported improving light trapping and conversion efficiency of a solar cell by modifying and randomly distributing ZnO nanorods. Carrier mobility is the central issue for optoelectronic semiconducting materials. However, there is rare information about quantitative analysis of the carrier mobility of $CH_3NH_3SnX_3$ theoretically.

In this work, we investigate the electronic properties, including the effective mass values of hole and electron at the Γ point. According to the calculated effective mass values, we further predict the charge mobility for nontoxic methylammonium tin halide ($CH_3NH_3SnI_3$) at the equilibrium geometry by using the Heyd–Scuseria–Ernzerhof (HSE06) hybrid functional method.[15] We also clarify the relationship between the carrier mobility anisotropy and electron occupation anisotropy in p orbit of Sn and I atoms to offer constructive guidance to tune the carrier mobility along a certain direction in future.

2. Computational details

In this work, first-principles computations on the basis of density functional theory (DFT) are performed in the orthorhombic phase of $MASnI_3$ lattice by using the Vienna ab initio simulation package (VASP).[16] Projector-augmented plane wave (PAW) approach is used to describe the ion–electron interactions.[17,18] We used the generalized gradient approximation (GGA) involving Perdew–Burke–Ernzerhof (PBE) functional and the Grimme vdW correction, which can accurately describe the weak interactions.[19,20] A cutoff energy of 400 eV for the plane-wave basis set is adopted in all computations. The k-point mesh of the Brillouin zone is set to be 4×4×4 for geometry optimization. The convergence threshold for self-consistent-field iteration is set to be 10^{-6} eV, and the atomic positions are fully optimized until all components of the residual forces are smaller than 0.001 eV/Å. The density of states (DOS) of perovskite $CH_3NH_3SnI_3$ is calculated by using the tetrahedron method with Blöchl corrections.[17] As is well known, the standard DFT usually underestimates the band gap of semiconductor due to the inherent lack of derivative discontinuity and the self-correlation error of electrons.[21] Yuan *et al.*[22] reported that the band gap for cubic phase of $CH_3NH_3SnI_3$ is just 0.244 eV, which underestimates about 1 eV compared with the experimental data (1.3 eV). To account for the underestimation of the band gap in standard DFT calculations, the accurate electronic structures are then calculated by using the Heyd–Scuseria–Ernzerhof (HSE06) hybrid functional.[15] The scalar-relativistic effects are included in the PAW Pseudopotentials. In addition, we realize that strong spin–orbit coupling (SOC) effects play a significant role in reducing the band gaps of compounds consisting of heavy elements. However, according to Bernal and Yang's work,[23] we can ignore SOC effects in Sn-based perovskites. So, the band calculated by the HSE06 methods does not consider the spin–orbit coupling (SOC). As is well known, the more serious distortion may induce stronger ferroelectricity, which might play a vital role in the high carrier mobility. So, we use an orthorhombic cell to approximate the realistic structure. We start our calculations by focusing on the orthorhombic phase of $CH_3NH_3SnI_3$,[24] as shown in Fig. 1. Based on the calculated band structures, we calculate the effective mass values along three different directions by fitting the band edge according to the following equation:

$$E(\boldsymbol{k}) = E\boldsymbol{k}_0 \pm \frac{\hbar^2}{2}[\boldsymbol{k}_i - \boldsymbol{k}_0][S_{ij}][\boldsymbol{k}_j - \boldsymbol{k}_0], \tag{1}$$

where $E(\boldsymbol{k}_0)$ represents the energy at the band extreme, that is, the value at the $\boldsymbol{k}_0$ in the Brillouin zone. The tensor S_{ij} is related to the effective mass tensor m^*_{ij} by

$$S_{ij} = \sum_{i=1}^{3}\sum_{i=1}^{3}\frac{1}{m^*_{ij}}, \tag{2}$$

where the total effective mass m^* can be computed from $m^* = 1/S_{ij}$. For orthorhombic Γ structures, the band extreme is located at the Γ point, thus, $\boldsymbol{k}_0 = 0$. Due to the symmetry of the crystal structure, the effective mass tensors of orthorhombic CH3NH3SnX_3 (X = Cl, Br, and I) have the following forms:

$$S_{ij}(\text{orthor hom bic}) = \begin{pmatrix} S_{11} & 0 & 0 \\ 0 & S_{22} & 0 \\ 0 & 0 & S_{33} \end{pmatrix}. \tag{3}$$

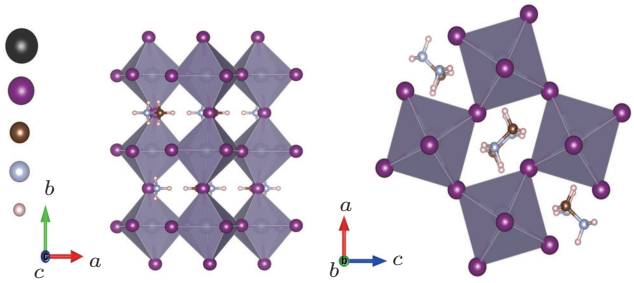

Fig. 1. (color online) Crystal structures of orthorhombic in $CH_3NH3SnI_3$ perovskite. The left panel is a side view, and the right panel shows the structure in polyhedron graphs (dark: tin; purple: iodine; brown: carbon; blue: nitrogen; pink: hydrogen).

In the matrix (Eq. (3)), the S_{11}, S_{22}, and S_{33} refer to the inverses of effective mass values of either the hole or electron in the [100], [010], and [001] directions, respectively. By fitting the obtained band dispersions in these three principal directions near the Γ point within Eq. (1), we compute the effective mass values of holes and electrons for orthorhombic

phase $CH_3NH_3SnI_3$. Based on the calculated effective mass values, the transport properties are evaluated theoretically using a simple approach based on the deformation potential theory as shown below[25]

$$\mu = \frac{(8\pi)^{1/2}\hbar^4 eC_{ii}}{3(m^*)^{5/2}(k_B T)^{3/2}E_1^2}, \quad (4)$$

where $\hbar$ is the reduced Planck constant, e is the element charge, C_{ii} is the elastic matrix constant, m^* is the effective mass of charge, k_B is the Boltzmann constant, T is the temperature, and E_1 is the deformation potential.[26–28] T is set to be room temperature ($T = 300$ K). Parameters m^*, E_1, and C_{ii} for $CH_3NH_3SnI_3$ can be acquired by first-principles computations, which can be obtained in Appendix A.

3. Results and discussion

3.1. A brief introduction to the structural properties

Like $MAPbX_3$, $MASnX_3$ also exhibits a very rich phase diagram as a function of temperature, i.e., the crystal structure goes from cubic, tetragonal, orthorhombic, and monoclinic to triclinic class by cooling.[17,23,27–29] Hao *et al.* reported a tetragonal $CH_3NH_3SnI_3$ phase at room temperature.[2] It was found that $CH_3NH_3SnI_3$ compound crystallizes into monoclinic phase at low temperature experimentally. However, the unit cell of monoclinic phase deviates from the orthorhombic crystal class very slightly.[28,29] The complicated phase transition behavior of $CH_3NH_3SnI_3$ is attributed to the disordering of $(CH_3NH_3)^+$ cations and the distortions of $(SnX_3)^-$ octahedra at finite temperature. The geometrical structure of the hybrid compound is illustrated in Fig. 1. In perovskite $CH_3NH_3SnI_3$, each Sn atom is surrounded by six I atoms, with four I atoms in the equatorial direction and two I atoms in the apical direction. The dipolar organic methylammonium ions are embedded in the octahedron SnI_6 cages. The previous work[30] revealed that $CH_3NH_3^+$ arrangements along different directions play an important role in the stability and electronic structure. Thus the wake interaction between inorganic and organic molecule must be taken into account as performed in VASP with the nonlocal vdW density functional. We first estimate the equilibrum lattice constants of the hybrid perovskite compound by using DFT + D2 calculations in the frame of the PBE–GGA density functional, and the results are listed in Table 1, which are consistent with previous results obtained by Feng and Xiao.[12] Meanwhile, the calculated averaged bond length and the bond angles of Sn–I–Sn along the equatorial and apical direction are shown in Table 2, which are in agreement with previous results.[11] From Table 1, the calculated bond lengths of Sn–I for orthorhombic phase in $CH_3NH_3SnI_3$ perovskite are about 3.09 Å and 3.12 Å–3.13 Å which are consistent with the experimental data.[12] The corresponding Sn–I–Sn angles are 89.77° and 94.86° in the equatorial and the apical direction respectively. These results reveal that $CH_3NH_3SnI_3$ has more distorted structure than $CH_3NH_3PbI_3$, which may be the origin of ferroelectricity.

Table 1. Lattice constants of orthorhombic phase in perovskite $CH_3NH_3SnI_3$ compared with Feng and Xiao's work.[12]

Compound	This work/Å			Feng and Xiao's work		
	a	*b*	*c*	*a*	*b*	*c*
orthorhombic	8.56	12.41	8.43	8.556	12.428	8.326

3.2. Electronic properties of $CH_3NH_3SnI_3$

For orthorhombic phase in perovskite $CH_3NH_3SnI_3$, the energy band structure is shown in Fig. 2, and the calculated energy band gap is 1.27 eV by using HSE06 functional method as shown in Table 2. Our calculations reveal that the $CH_3NH_3SnI_3$ is a direct gap semiconductor, and the calculated results are consistent with those reported in previous research.[31] Figures 2(a) and 2(b) show the band structures of the orthorhombic phase in $CH_3NH_3SnI_3$ calculated by standard DFT and HSE06 functional methods respectively. For this phase, they all exhibit a direct band gap at the Γ point of the Brillouin zone. The difference could be seen easily from Figs. 2(a) and 2(b), the calculated band gaps are 0.74 eV by standard density functions theory and 1.27 eV by HSE06 method, respectively, which are listed in Table 2.

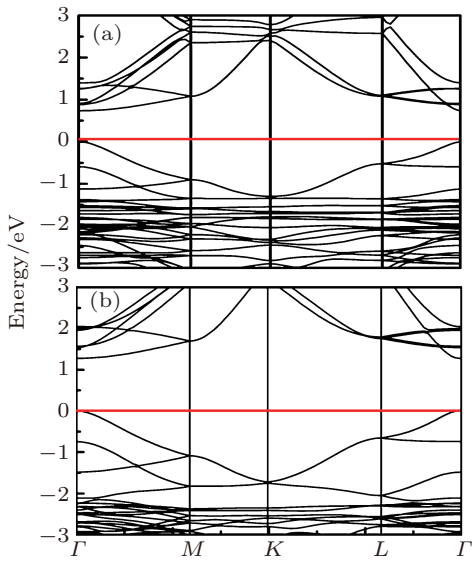

Fig. 2. (color online) Band structures for orthorhombic phase in $CH_3NH_3SnI_3$ perovskites by standard DFT and HSE06 calculations, respectively. The Brillouin zone is also shown.

Table 2. Calculated band gaps of DFT-D2 and HSE06, the bond lengths of Sn–I and the bond angles of Sn–I–Sn along the equatorial and apical direction.

Band gap/eV		Sn–I–Sn bond angel/(°)		Bond lengths of Sn–I/Å	
DFT-D2	HSE06	equatorial	apical	Cal. cell	Exp. cell
0.74	1.27	89.78	94.86	3.09-3.14	3.09-3.19

As is well known, the standard DFT usually underestimates the band gap of semiconductors due to the inherent lack of derivative discontinuity and the self-correlation error

of electrons.[32] Therefore, results (1.27 eV) obtained by the hybrid functional within the framework of density functional theory (DFT-D2) method are closer to the experimental data (1.3 eV).[9] We ascribe the difference between the calculated data and experimental data to the following reasons: (i) the experimental materials are flawed, while the calculated structure is considered as an ideal model; (ii) though HSE06 calculations improve the exchange action, the improved exchange effect is still from a semi-empirical theory. According to the calculated band structure, the carrier effective mass values are shown in Table 3. The effective mass values of orthorhombic phase in perovskite $CH_3NH_3SnI_3$ at Γ along three principal directions, i.e., [1 0 0], [0 1 0], and [0 0 1] direction are evaluated respectively by using Eq. (1) as the effective mass values of hole and electron are associated with the slope of the band edge. The calculated results compared with those of Feng's work are listed in Table 3. From the Table 3, it is clearly seen that carrier effective mass values along three principal directions are anisotropic, which are consistent with Feng and Xiao's[12] results. Owing to our calculated band gap more closer to the experimental data, we believe that the effective mass values of electrons and holes are considered as more reliable results. Also, the results reveal that the orthorhombic phase in $CH_3NH_3SnI_3$ shows that the hole effective mass is smaller than the electron's.

Table 3. Calculated effective mass values of hole and electron of $CH_3NH_3SnI_3$ for orthorhombic phase compared with the results of $CH_3NH_3SnI_3$ (orthorhombic phase) calculated by Feng and Xiao's work.[12]

	Direction	m_e^*/m_0	m_e^*/m_0[11]	m_h^*/m_0	m_e^*/m_0[11]
Orthorhombic	x	1.77	3.74	0.35	0.59
	y	0.15	0.81	0.11	1.14
	z	1.75	5.77	0.26	0.53

The density of states (DOS), and the projected density of states (PDOS) of $CH_3NH_3SnI_3$ are shown in Fig. 3. The calculated results show that the valence band maximum (VBM) for orthorhombic phase in $CH_3NH_3SnI_3$ is mainly due to the 5p orbitals of the I and partly due to the 5s orbital of Sn, while in the conduction band minimum (CBM), the main contribution is from the 5p orbitals of Sn and little contribution is from the 5p orbitals of I. Also, it is noted that the organic cations $(CH_3NH_3)^+$ are far from the Fermi level. Therefore, the emergency of the photocurrent is mainly generated by the electron transition from 5p orbitals of I and 5s orbital of Sn to the 5p orbitals of Sn. A similar structure such as $CH_3NH_3PbI_3$ also shows that the strong hybridization of s–p orbital in valence band maximum (VBM) plays an important role in the structure stability and the small effective mass.[24] More detailed analyses of the chemical bonding mechanisms of those hybrid organic–inorganic pervoksite materials can be found in previous publications.[33–36]

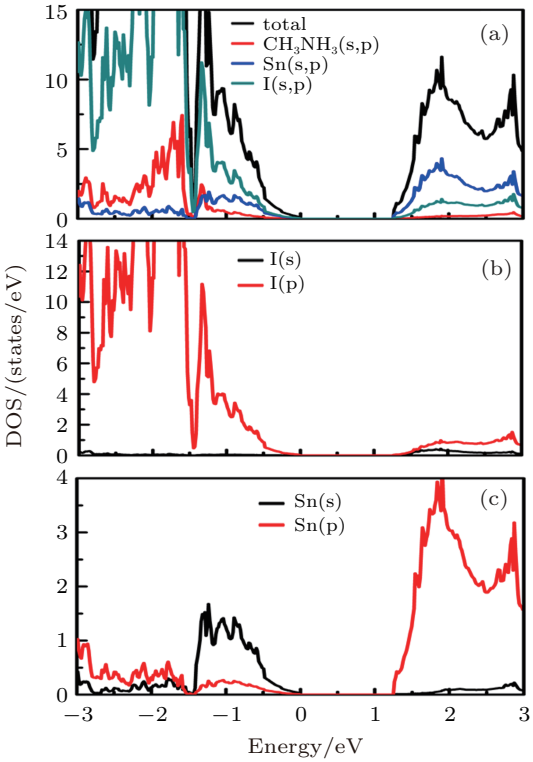

Fig. 3. (color online) The calculated PDOS from top to bottom in $CH_3NH_3SnI_3$ perovskite.

In order to further illustrate our results, the calculated projected DOS in valence band maximum and conduction band minimum are shown in Fig. 4 to explain the electron and hole carrier effective mass values along three principal directions. Here, we present the theoretical discovery of a new relationship between the carrier effective mass anisotropy and the electronic DOS anisotropy along three principal directions. As mentioned above, the valence band maximum (VBM) is mainly due to the I-p states and the conduction band minimum (CBM) is mainly due to the Sn-p states. Thus we just discuss the electron occupation probabilities of I-p states in valence band maximum and Sn-p states in conduction band minimum, respectively, as shown in Fig. 4. The above Table 2 reveals that the hole effective mass values of orthorhombic phase in $CH_3NH_3SnI_3$ along the x, y, and z directions are 0.35, 0.11, and 0.27 respectively. From Fig. 4(a), increasing sequence of hole effective mass values along different directions is $m^*_{[100]} > m^*_{[010]} > m^*_{[100]}$, which is consistent with the decreasing sequence of electron occupation probabilities in the p orbital of I along the x, y, and z directions $p_x < p_z < p_y$ in valence band maximum. Similarly the calculated values of electron effective mass $m^*_{[100]}$, $m^*_{[010]}$, and $m^*_{[001]}$ are 1.77, 0.15, and 1.75 respectively. Increasing sequence of electron effective mass values along different directions is $m^*_{[100]} > m^*_{[100]} > m^*_{[010]}$, which is also consistent with

the decreasing sequence of electron occupation probabilities in the p orbital of Sn along the x, y, and z directions as follows: $p_y > p_z > p_x$ in the bottom conduction-band depicted in Fig. 4(b). There might be such a relationship that the higher the occupation probabilities in the p orbital along the x, y, and z directions, the smaller the effective mass is, hence the higher the carrier mobility.

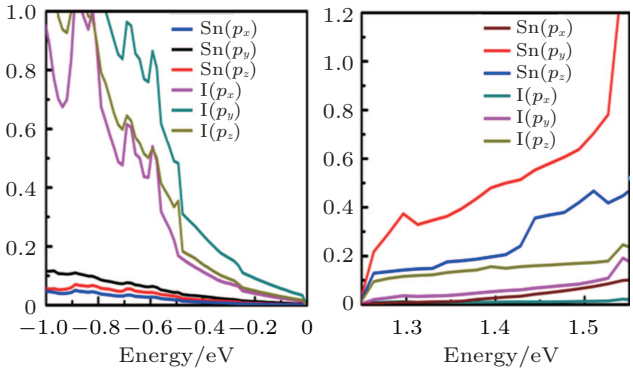

Fig. 4. (color online) Detailed PDOS from top to bottom for orthorhombic phase in $CH_3NH_3SnI_3$ perovskite. The left panel shows the VBM, and the right panel shows the CBM.

3.3. High mobilities of electrons and holes

In order to evaluate the transfer efficiency of the carrier in perovskite $CH_3NH_3SnI_3$, we systematically investigate the carrier mobility of $CH_3NH_3SnI_3$. From experimental measurement, the system of $CH_3NH_3SnI_3$ was reported to have high electron mobility ($\mu_e \sim 2320$ cm^2·V^{-1}·s^{-1}),[8] which is higher than $CH_3NH_3PbI_3$ ($\mu_e \sim 66$ cm^2·V^{-1}·s^{-1}).[8] The charge mobility is calculated according to Eq. (2). It should be noticed that reliable band structure is highly essential for the calculations of carrier mobilities. All the calculated results are listed in Table 4. Figure S1 (see Appendix A) shows the energy changes of VBM and CBM band edge of $CH_3NH_3SnI_3$ with the applied strain along the x, y, and z directions, respectively. By simulating the linear relation between band edge energy (E_{edge}) and strain (δ) exerted in the x, y, and z directions, we can obtain the deformation potential (DP) constant E_1. The DP constant is a characterization of the coupling strength of the electron or hole to the acoustic phonon. It is found that the DP constant E_1 values of electrons and holes are comparable in $CH_3NH_3SnI_3$ perovskite (see Table 4). The elastic matrix constant along the y direction is 637 kbar (1 bar =10^5 Pa), which is about twice that along the z direction, and the effective mass values for the hole and electron are the minimal (along z direction) among three directions. Therefore, it is clearly seen that the carrier mobility along the y direction is highest because of high DP and small effective masses. From Eq. (2), we can see the main difference between the electron and hole mobilities in $CH_3NH_3SnI_3$ derives from the small effective masses, rather than the DP constant E_1. It can be clearly seen that $CH_3NH_3SnI_3$ perovskite shows high carrier mobilities of 14470 cm^2·V^{-1}·S^{-1} and 5445 cm^2·V^{-1}·S^{-1} for holes and electrons, respectively, which are rather higher than the experimental data (2230 cm^2·V^{-1}·S^{-1}).[8] The difference can be attributed to the following reasons: (i) there are inevitably impurities and defects in the experimental material; (ii) the phonons have little influence on the charge transport properties at low temperatures; (iii) the Sn^{2+} ion can be oxidized into Sn^{4+} state easily, which may underestimate the carrier mobilities in the experimental measurement. The carrier mobility (17 and 545, 11 and 1663 cm^2·V^{-1}·S^{-1}) for holes and electrons in the x and z direction are two or three orders lower than that along the y direction, respectively, and so is the anisotropic carrier mobility. Our calculated carrier mobility may lay the solid foundation and the theoretical support for the application of the device.

Table 4. Calculated values of deformation potentials E_{1c} and E_{1v} for electron and hole, respectively, elastic constant (c_{ii}), and carrier mobilities μ_e and μ_h for electron and hole, respectively at the Γ point of the Brillouin zone. Three directions are considered for the orthorhombic phase.

	Direction	E_{1c}/eV	E_{1v}/eV	C_{ii}/kbar	$\mu_e/10^3$ cm^2·V^{-1}·S^{-1}	$\mu_e/10^3$ cm^2·V^{-1}·S^{-1}
Orthorhombic	x	–6.25	–8.23	432	0.017	0.545
	y	–9.13	–8.26	637	5.445	14.47
	z	–7.39	–6.13	382	0.011	1.663

4. Conclusions

In this work, we employ DFT + D2 and HSE06 to study the equilibrium lattice parameters, electronic structures and the intrinsic charge carrier mobility of orthorhombic phase in $CH_3NH_3SnI_3$. We conclude that $CH_3NH_3SnI_3$ is semiconductor with direct band gaps at the Γ point. The anisotropy of carrier effective mass can be attributed to the anisotropy of electron occupation probabilities along the three principal directions, so can the anisotropy of carrier mobility. The results reveal that the high carrier mobility is ascribed to the intrinsically small effective mass, in addition to a relatively weak electron–phonon coupling. Owing to the hole mobility higher than the electron mobility, the $CH_3NH_3SnI_3$ perovskite can be considered as p-type semiconductor in electrical conduction. The suitable energy bad gaps and impressively large carrier mobilities reported here indicate that $CH_3NH_3SnI_3$ is a very promising material in the field of application and designing

for solar cell devices.

Appendix A

According to the band structure of the equilibrium point, we can fit two curves for the top valence band and the bottom conduction band near Γ point, so we obtain the effective mass m_h and m_e for electron and hole along three directions, respectively. The deformation potential (E_1) is defined as the energy shift of the band energy position (ΔE) with respect to a small lattice dilation (Δl) along a lattice (l_0) direction, i.e., $E_1 = \Delta E/(\Delta l/l_0)$. Then, we calculate the band structure of unit cells at five chosen deformed lattice constants: $0.99a_0$, $0.995a_0$, a_0, $1.005a_0$, $1.01a_0$. From the variations of the bottom conduction band and the top valence band with Δ, we obtain two straight lines with correlation coefficient > 0.999, and from the slopes of these straight lines we obtain E_{1v} and E_{1c} as shown in Fig. S1.

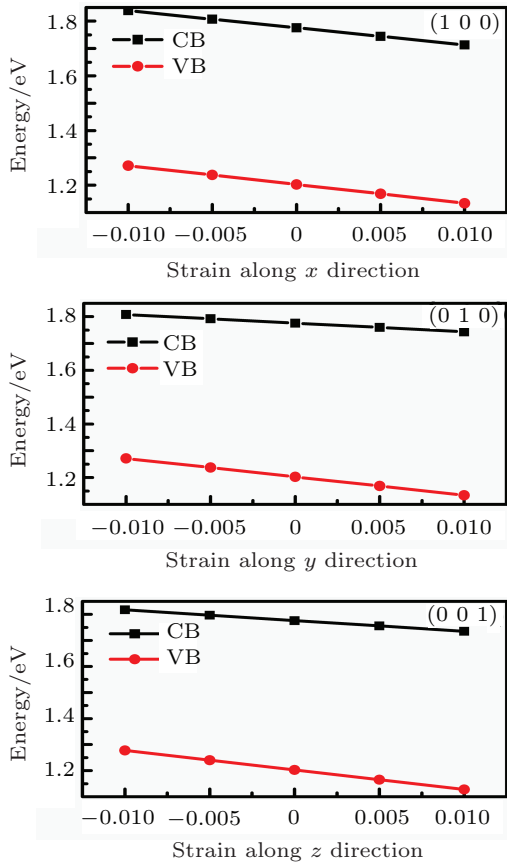

Fig. S1. (color online) Band-edge positions of VB and CB with respect to the lattice dilation $\Delta l/l_0$ along the direction for the $CH_3NH_3SnI_3$. Solid lines represent the linear fit, which defines DP constant.

The effective mass of the hole or electron at the band extreme is related to the band dispersion by

$$E(\boldsymbol{k}) = E(\boldsymbol{k}_0) \pm \frac{\hbar^2}{2}[\boldsymbol{k}_i - \boldsymbol{k}_0][S_{ij}][\boldsymbol{k}_j - \boldsymbol{k}_0], \qquad \text{(A1)}$$

where $E(\boldsymbol{k}_0)$ represents the energy at the band extreme, that is, the value at $\boldsymbol{k}_0$ in the Brillouin zone. The tensor S_{ij} is related to the effective mass tensor m^*_{ij} by

$$S_{ij} = \sum_{i=1}^{3}\sum_{i=1}^{3}\frac{1}{m_{ij}*}, \qquad \text{(A2)}$$

where the total effective mass M^* can be computed from $M^* = 1/S_{ij}$. For orthorhombic Γ structure, the band extreme is located at Γ point. Thus, $\boldsymbol{k}_0 = 0$. Due to the symmetry of the crystal structure, the effective mass tensors of orthorhombic $CH_3NH_3SnX_3$ (X = Cl, Br and I) have the following form

$$S_{ij}(\text{orthor hom bic}) = \begin{pmatrix} S_{11} & 0 & 0 \\ 0 & S_{22} & 0 \\ 0 & 0 & S_{33} \end{pmatrix}. \qquad \text{(A3)}$$

In the matrix (Eq. (A3)), the S_{11}, S_{22}, and S_{33} refer to the inverse effective mass of either the hole or electron in the [100], [010], and [001] directions, respectively. By fitting the obtained band dispersions in these three principal directions near the Γ point in Eq. (1), we compute the effective mass values of holes and electrons for orthorhombic phase $CH_3NH_3SnI_3$ as shown in Table 2.

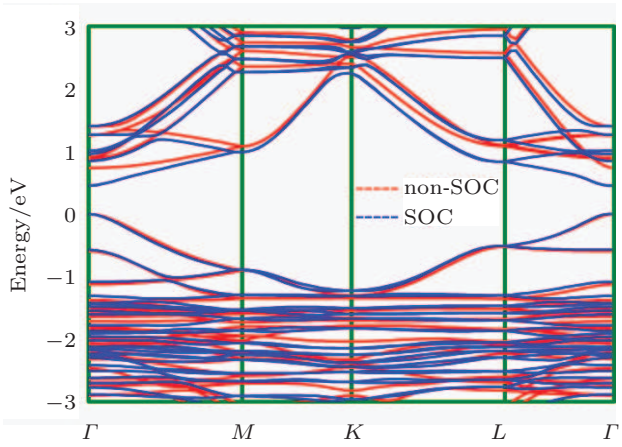

Fig. S2. (color online) Band structures of $CH_3NH_3SnI_3$ (without and with spin–orbit (SOC)) obtained using DFT–PBE calculations. The red line corresponds to non-SOC (without SOC), and the blue line refers to SOC (with SOC).

We performed PBE+SOC calculation to compare with the PBE calculation as shown in Fig. S2. From Fig. S2, the band gap for PBE + SOC calculation is about 0.25 eV less than that for standard PBE calculation, which is consistent with the previous calculated results (Bernal C and Yang K 2014 *J. Phys. Chem. C* **118** 24383). We can also see that the band dispersions seem to be identical. There may be a controversy over the fact that SOC cannot be ignored in Sn-based perovskites. Moreover, the previous calculations for the material of $CH_3NH_3PbI_3$ show that the effective mass values of the electron and hole are 0.19, 0.17, 0.18 and 0.28, 0.25, 0.28 for the calculation with the SOC–GW, SOC–DFT, and non–SOC method, respectively (Bernal C and Yang K 2014 *J. Phys. Chem. C* **118** 24383). As is well known, Pb is a heavy metal

element, the calculated results of band gap for the material of $CH_3NH_3PbI_3$ show a significant difference (about 1.1 eV) between the non-SOC and SOC effects. This shows that the SOC calculation has little influence on the electron and hole mass in spite of the influence on band gap. The researchers (Geng W, Zhang L, Zhang Y N, Lau W M and Liu L M 2014 *J. Phys. Chem. C* **118** 19565) also mentioned that Sn-based perovskite could ignore the SOC effects. On the other hand, our calculated band gap (1.27 eV) is closer to experimental data (1.3 eV). Therefore, we think that the SOC calculations have little influence on our calculated results.

Acknowledgment

The authors express their thanks to the Changsha Supercomputer Center for computation.

References

[1] Chung I, Lee B, He J Q, Chang R P H and Kanatzidis M G 2012 *Nature* **485** 486
[2] Hao F, Stoumpos C C, Cao D H, Chang R P H and Kanatzidis M G 2014 *Nat. Photon.* **8** 489
[3] Kojima A, Teshima K, Shirai Y and Miyasaka T J 2009 *Am. Chem. Soc.* **131** 6050
[4] Kim H S, Lee C R, Im J H, Lee K B, Moehl T, Marchioro A, Moon S J, Humphry-Baker R, Yum J H, Moser J E, Gratzel M and Park N G 2012 *Sci. Rep.* **2** 11203
[5] Lee M M, Teuscher J, Miyasaka T, Murakami T N and Snaith H J 2012 *Science* **338** 643
[6] Gidlow D A 2004 *Occup. Med-Oxford* **54** 76
[7] Aslihan B, Dinh D T, Anitha E, Jean M, Marc M, Hans-Gerd B and Bert C 2016 *Sci. Rep.* **6** 18721
[8] Zhao Y Q, Wu L J, Wang L Z, Liu B, He P B and Cai M Q 2016 *J. Power Source* **313** 96
[9] Stoumpos C C, Malliakas C D and Kanatzidis M J 2013 *Inorg. Chem.* **52** 9019
[10] papaassiliou G C and Koutselas I B 1995 *Synthetic Met.* **71** 1713
[11] Lang L, Yang J H, Liu H R, Xiang H J and Gong X G 2014 *Phys. Lett. A* **378** 290
[12] Feng J and Xiao B 2014 *J. Phys. Chem. C* **118** 19655
[13] Umari P Mosconi E and De Angelis F 2014 *Sci. Rep.* **4** 563
[14] Jia Z N, Zhang X D, Liu Y, Wang Y F, Fan J, Liu C C and Zhao Y 2014 *Chin. Phys. B* **23** 046106
[15] Heyd J, Scuseria G E and Ernzerhof M 2003 *J. Chem. Phys.* **118** 8207
[16] Kresse G and Hafner J 1993 *Phys. Rev. B* **47** 558
[17] Blöchl P E, Jepsen O and Andersen O K 1994 *Phys. Rev. B* **50** 17953
[18] Kresse G and Joubert D 1999 *Phys. Rev. B* **59** 1758
[19] Perdew J P, Burke L and Ernzerhof M 1996 *Phys. Rev. Lett.* **77** 3865
[20] Grimme S 2006 *J. Comput. Chem.* **27** 1787
[21] Takahashi Y, Obara R, Lin Z Z, Takahashi Y, Naito T, Inabe T, Ishibashi S and Terakura K 2011 *Dalton T.* **40** 5563
[22] Yuan Y, Xu R, Xu H T, Hong F, Xu F and Wang L J 2015 *Chin. Phys. B* **24** 116302
[23] Bernal C and Yang K 2014 *J. Phys. Chem. C* **118** 24383
[24] Feng J and Xiao B 2014 *J. Phys. Chem. Lett.* **5** 1719
[25] Chung I, Song J H, Im J, Androulakis J, Malliakas C D, Li H, Freeman A J, Kenney J T and Kanatzidis M G 2012 *J. Am. Chem. Soc.* **134** 8579
[26] Wei S H and Zunger A 1998 *Phys. Rev. B* **60** 5404
[27] Li Y H, Gong X G and Wei S H 2006 *Appl. Phys. Lett.* **88** 4520
[28] Franceschetti A, Wei S H and Zunger A 1994 *Phys. Rev. B* **50** 17797
[29] Wallentin J, Anttu N, Asoli D, Huffman M, Aberg I, Magnusson M H, Siefer G, Fuss-Kailuweit P, Dimroth F Witzigmann B, Xu H Q, Samuelson L, Deppert K and Borgstrom M T 2013 *Science* **339** 1057
[30] Geng W, Zhang L, Zhang Y N, Lau W M and Liu L M 2014 *J. Phys. Chem. C* **118** 19565
[31] Kresse G and Furthmüller J 1996 *Mater. Sci.* **6** 15
[32] Bardeen J and Shockley W 1950 *Phys. Rev.* **80** 72
[33] Kawamura Y, Mashiyama H and Hasebe K 2002 *J. Phys. Soc. Jpn.* **71** 1694
[34] Yin W J Shi T T and Yan Y F 2014 *Adv. Mater.* **26** 4653
[35] Wang Y, Gould T, Dobson J F, Zhang H M Yang H G, Yao X D and Zhao H J 2014 *Phys. Chem. Chem. Phys.* **16** 1424
[36] Huang L Y and Lambrecht W R L 2013 *Phys. Rev. B* **88** 1702